Advanced Energy Materials

ADVANCED ENERGY MATERIALS
www.advenergymat.de

RESEARCH ARTICLE

Heterocycle-Bridged Short Sulfur-Chain Polymers for Polysulfide-Suppressing Cathodes in Lithium-Organosulfide Batteries

Xingkai Ma | Huan Li | Junchuan Liang | Yaoda Wang | Tianyu Shen | Xinmei Song | Zuoao Wu | Huaizhu Wang | Lina Qin | Tianchen Yu | Zuoxiu Tie | Zhong Jin

State Key Laboratory of Coordination Chemistry, MOE Key Laboratory of Mesoscopic Chemistry, MOE Key Laboratory of High Performance Polymer Materials and Technology, Jiangsu Key Laboratory of Green Energy Catalysis and Intelligent Chemical Engineering, Suzhou Key Laboratory of Green Intelligent Manufacturing of New Energy Materials and Devices, Tianchang New Materials and Energy Technologies Research Center, Institute of Green Chemistry and Engineering, School of Chemistry and Chemical Engineering, Nanjing University, Nanjing, Jiangsu, China

Correspondence: Zhong Jin (zhongjin@nju.edu.cn)

Received: 11 November 2025 | **Revised:** 9 January 2026 | **Accepted:** 19 January 2026

Keywords: heterocycle-bridged | lithium-organosulfide batteries | polysulfide-suppressing | short sulfur-chain polymers

ABSTRACT

Organosulfur polymers, valued for their structural tunability and environmental friendliness as cathode materials for lithium-sulfur (Li-S) batteries, face challenges in practical applications due to inadequate cycling stability and rate performance. Herein, we report the rational design and green synthesis of a heterocycle-bridged short sulfur-chain polymer, namely poly(pyrazine tetrasulfide) (PPZTS), with a sulfur-rich atomic chain structure as a high-performance cathode material for lithium-organosulfide batteries. The pyrazine-bridged short sulfur-chain structure in PPZTS prevents the formation and shuttling of long-chain polysulfides, and the electronegative π-conjugated pyrazine rings facilitate uniform Li^+ diffusion, leading to significant improvements in both cycling stability and rate performance. The PPZTS cathode achieves a high capacity of 1250 mAh g^{-1} at 0.1 A g^{-1} and 660 mAh g^{-1} at 5.0 A g^{-1}. When cycled at 1.0 A g^{-1}, the PPZTS cathode demonstrates an initial capacity of 850.9 mAh g^{-1} and retaining 630.4 mAh g^{-1} after 400 cycles. The PPZTS cathode also demonstrates robust performance across a wide temperature range from −20 to 80°C, and the deployment in soft-packed batteries further suggests its potential practicability. This work underscores the intriguing potential of heterocycle-linked short sulfur-chain polymers as cathode materials for alkali metal-organosulfide batteries, addressing key challenges in organosulfur polymer applications for advanced energy storage devices.

1 | Introduction

Lithium-sulfur (Li-S) batteries have garnered considerable attention owing to their exceptional theoretical energy density (2600 Wh kg^{-1}), cost effectiveness, and eco-friendly nature [1–9]. However, several challenges hinder their commercial viability, including the inherent electronic insulation of sulfur, the shuttle effect of polysulfide intermediates, and substantial volume expansion during lithiation [10–16]. Extensive research has been undertaken to enhance the performance of Li-S batteries, mainly focusing on two primary strategies to confine sulfur species within the cathode. The first approach involves encapsulating

Xingkai Ma and Huan Li contributed equally to this work.

elemental sulfur within carbon-based nanomaterials or inorganic matrices [17–20]. These composites have shown improved cycling stability and rate performance to some extent. However, practical applications are still limited due to factors such as low sulfur utilization, formation of insulating sulfur species, and generation of long-chain polysulfides. These long-chain polysulfides can shuttle between the cathode and anode, leading to the loss of active sulfur and capacity. The alternative strategy is to form organosulfur compounds by covalently bonding sulfur with organic molecules or polymer chains, thus providing high sulfur content and mitigating the shuttle effect [21–29]. The tunable molecular structure and functional groups of organosulfur materials enable diverse electrochemical properties. However, a long sulfur-chain would result in diminished electrical conductivity, which limits rate performance, and cannot fully prevent the shuttle effect, thus compromising the cycling stability of lithium-organosulfide batteries. Therefore, there is an urgent need to develop advanced organosulfur polymers with short sulfur-chain and optimized molecular structure to achieve high-performance Li-S batteries.

Herein, we report the rational design of an organosulfur polymer, namely poly(pyrazine tetrasulfide) (PPZTS), synthesized via the substitution of chlorine in dichloropyrazine (DCPZ) with a short sulfur-chain (Figure 1). The unique pyrazine-bridged short sulfur-chain structure of PPZTS efficiently avoids the shuttle effect and facilitates lithium-ion transport, as the short sulfur-chain prevents the formation and shuttling of long-chain polysulfides, while the electron-rich π-conjugation pyrazine units promote lithium-ion diffusion. Additionally, the polar nitrogen sites in the pyrazine ring provide strong interactions with charge-discharge intermediates and immobilize lithium sulfide species, thus enhancing electrochemical stability. These structural features collectively contribute to the high discharge capacity, rate capability, and cycling stability of lithium-organosulfide batteries. As a result, the PPZTS cathode exhibits a substantial specific capacity of approximately 1250 mAh g^{-1} at 0.1 A g^{-1} and good capacity retention of 660 mAh g^{-1} at 5.0 A g^{-1}. Additionally, it demonstrates a high specific capacity of 850.9 mAh g^{-1} at 1.0 A g^{-1} and preserves a value of 630.4 mAh g^{-1} after 400 cycles. These findings highlight the great potential of heterocycle-bridged short sulfur-chain organosulfur polymers to serve as cathode materials for high-capacity and long-lifespan alkali metal-organosulfide batteries.

2 | Result and Discussion

The short sulfur-chain organosulfur polymer, PPZTS, was synthesized via a substitution reaction between dichloropyrazine (DCPZ) and Na_2S_4 (Figure 1a). With a high content of S atoms, PPZTS facilitates a higher density of lithium storage sites and possesses a high theoretical specific capacity of 1256.5 mAh g^{-1}. Figure 1b presents the schematic working mechanism of PPZTS as a cathode material for lithium-organosulfur batteries. Due to the short sulfur-chain length in PPZTS, polysulfides are not formed during the discharge process. Instead, Li^+ ions react with sulfur sites in the polymer matrix to generate pyrazine-based lithium organosulfide (PZS-Li) and Li_2S, inhibiting the formation of soluble long-chain polysulfides and thus preventing the shuttle effect. In addition, the polymer backbone incorporates electron-withdrawing pyrazine rings, which improve electron delocalization and provide lithophilic sites via nitrogen–lithium interactions, providing a certain adsorption affinity for the PZS-Li and Li_2S generated in the adjacent region and facilitating uniform Li^+ distribution. Furthermore, the rigid conjugated framework and strong S–C bonds ensure structural integrity and low sulfur dissolution during cycling, contributing to high capacity retention and long-term stability.

The morphology and composition features of as-prepared PPZTS were investigated by scanning electron microscope (SEM) and energy dispersive X-ray spectroscopy (EDX) (Figure 1c–e). As observed from the SEM images, the PPZTS material exhibits an irregular block-like morphology with relatively uniform particle size distribution, dense surfaces, and well-defined structural integrity. Such morphology is favorable for electrolyte penetration and facilitates efficient lithium-ion diffusion. EDX mapping reveals a uniform distribution of S element throughout the PPZTS structure with no obvious aggregation, indicating a homogeneous incorporation of sulfur at the molecular level. EDX analysis reveals that the atomic ratio of carbon to sulfur in PPZTS is approximately 1:1.09, which is consistent with the designed short sulfur-chain-rich molecular framework. Furthermore, the supplementary elemental analysis results provided in Table S1 further corroborate a C/S atomic ratio close to 1:1.01. This indicates that the sulfur atoms are covalently bonded to the pyrazine rings in the form of short sulfur chains (C–S_4–C), forming a stable organosulfur framework. The high sulfur content provides abundant reversible redox-active sites, which is a key prerequisite for achieving high specific capacity. By comparing the XRD results of PPZTS and sulfur powder, it could be confirmed that the existence form of S atoms in PPZTS has a distinct variation (Figure S1). Unlike the clear crystalline peaks of elemental sulfur, the XRD pattern of PPZTS exhibits only a broad hump from 15° to 30°, indicating the presence of a polymeric structure [30].

The structural characterizations of DCPZ precursor and as-synthesized PPZTS sample were carried out through Fourier transform infrared (FTIR), Raman, and X-ray photoelectron spectroscopy (XPS) analyses. The FTIR spectrum of PPZTS (Figure 2a) shows an absorption peak at 1638 cm^{-1} corresponded to the C═C stretching vibration [31], while the peaks at 1350 and 1100 cm^{-1} represent the C═N and C–N stretching vibration, respectively [32]. These characteristic peaks are also present in the FTIR spectrum of DCPZ precursor, confirming the preservation of the conjugated pyrazine backbone after the reaction. Additionally, a strong peak at 710 cm^{-1} in the FTIR spectrum of DCPZ precursor is attributed to the C–Cl bond, which disappears in the FTIR spectrum of PPZTS. Instead, a new peak appears at 1250 cm^{-1}, corresponding to the C–S bond [33], and another peak at 610 cm^{-1} is assigned to the S–S bond stretching vibration [34]. The disappearance of C–Cl and the emergence of C–S and S–S bonds indicate the substitution and sulfurization during the synthesis process of PPZTS. These results suggest that PPZTS has been successfully synthesized from DCPZ precursor through specific functional group transformations. The characteristic structural units of DCPZ precursor, such as C═C and C═N moieties, are preserved in the product, while the emergence of new sulfur-related vibrational signals (C–S and S–S) confirms the formation

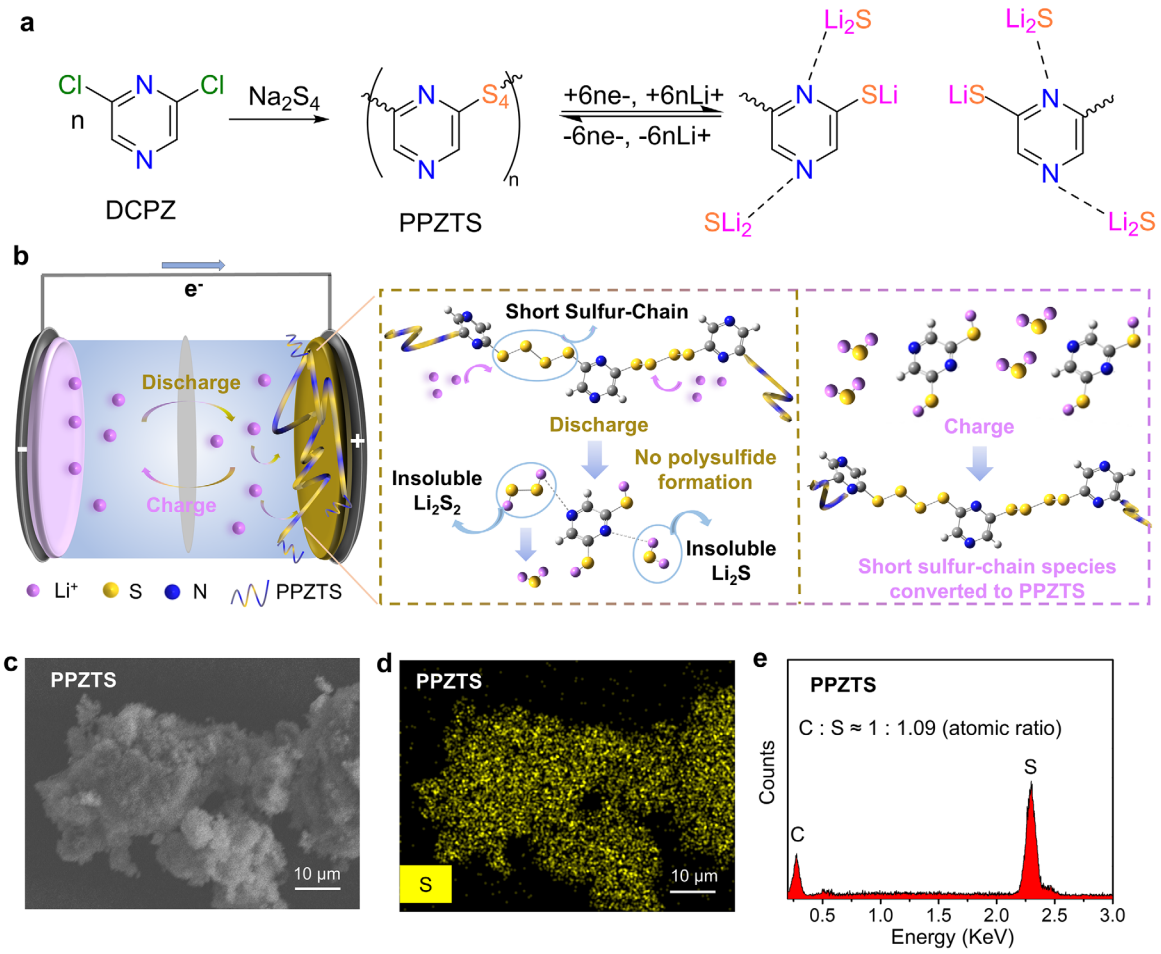

FIGURE 1 | Synthesis, characterizations, and working mechanism of PPZTS. (a) Synthesis route and Li^+ storage mechanism of PPZTS, demonstrating the avoidance of polysulfide formation and shuttle effect. (b) Schematic diagram of the working mechanism of PPZTS as a cathode material for the inhibition of the shuttle effect in lithium-organosulfide batteries. (c) SEM image, (d) corresponding S element mapping, and (e) EDX analysis result of PPZTS.

of the PPZTS. The Raman spectrum of DCPZ precursor presents a distinct peak at 1020 cm^{-1} corresponding to C–Cl stretching vibration (Figure 2b), which is substituted by the signals of C–S (450 cm^{-1}) and S–S (480 cm^{-1}) bonds in PPZTS [35]. XPS analyses were conducted to further determine the chemical compositions of both samples. The C 1s XPS spectrum (Figure 2c) of DCPZ precursor shows three deconvoluted peaks at 284.6, 285.2, and 286.2 eV, corresponding to the C═C, C–N, and C–Cl bonds, respectively [36]. In contrast, for PPZTS, the signal of C–S bond could be clearly observed at 285.6 eV [36]. Additionally, the S 2p XPS spectrum of PPZTS (Figure 2d) displays three well-defined peaks at 163.4, 165.0, and 168.2 eV, corresponding to C–S, S–S, and polarized sulfur environments, respectively [34, 36]. The appearance of these signals, which are absent in the DCPZ precursor, confirms the successful formation of covalent sulfur linkages and structural transformation during the synthesis of PPZTS.

The cyclic voltammetry (CV) curves of PPZTS cathode were recorded at a scan rate of 0.5 mV s^{-1} in the voltage range of 1.5–3.0 V vs. Li^+/Li (Figure 3a). The CV curves exhibit three distinct redox peaks that well overlapped during the subseqent cycles, indicating the presence of a reversible electrochemical reaction process for Li^+ storage and release. The two reduction peaks correspond to the storage of Li^+ in PZS-Li and the generation of Li_2S, respectively. Compared with the CV curves of traditional sulfur/carbon (S/C) composite cathode (Figure S2), the peak current intensities of PPZTS are sharper and higher, suggesting its higher electrochemical reaction activity. Figure 3b depicts the electrochemical impedance spectroscopy (EIS) results for the PPZTS cathode at the pristine state and after 100 cycles. Initially, the charge transfer resistance of the pristine PPZTS cathode is measured to be 129 Ω, indicating favorable electronic conductivity and efficient interfacial charge transport. Impressively, after 100 cycles, charge transfer resistance markedly decreases to 13 Ω, implying a significant enhancement in the electrode/electrolyte interface and overall charge transfer kinetics. This pronounced impedance reduction highlights the smooth charge transfer and robust electrochemical stability of PPZTS cathode during prolonged cycling. In contrast, the charge transfer resistance of the conventional S/C compsite cathode exceeds 300 Ω at pristine state (Figure S3a), and remains as high as 170 Ω after 100 cycles (Figure S3b), indicating sluggish charge transport and poor interfacial stability. Figure 3c shows the CV curves of PPZTS cathode at different scan rates ranging from 0.2 to 1.0 mV s^{-1}. As the scan rate increases, the response current of the PPZTS

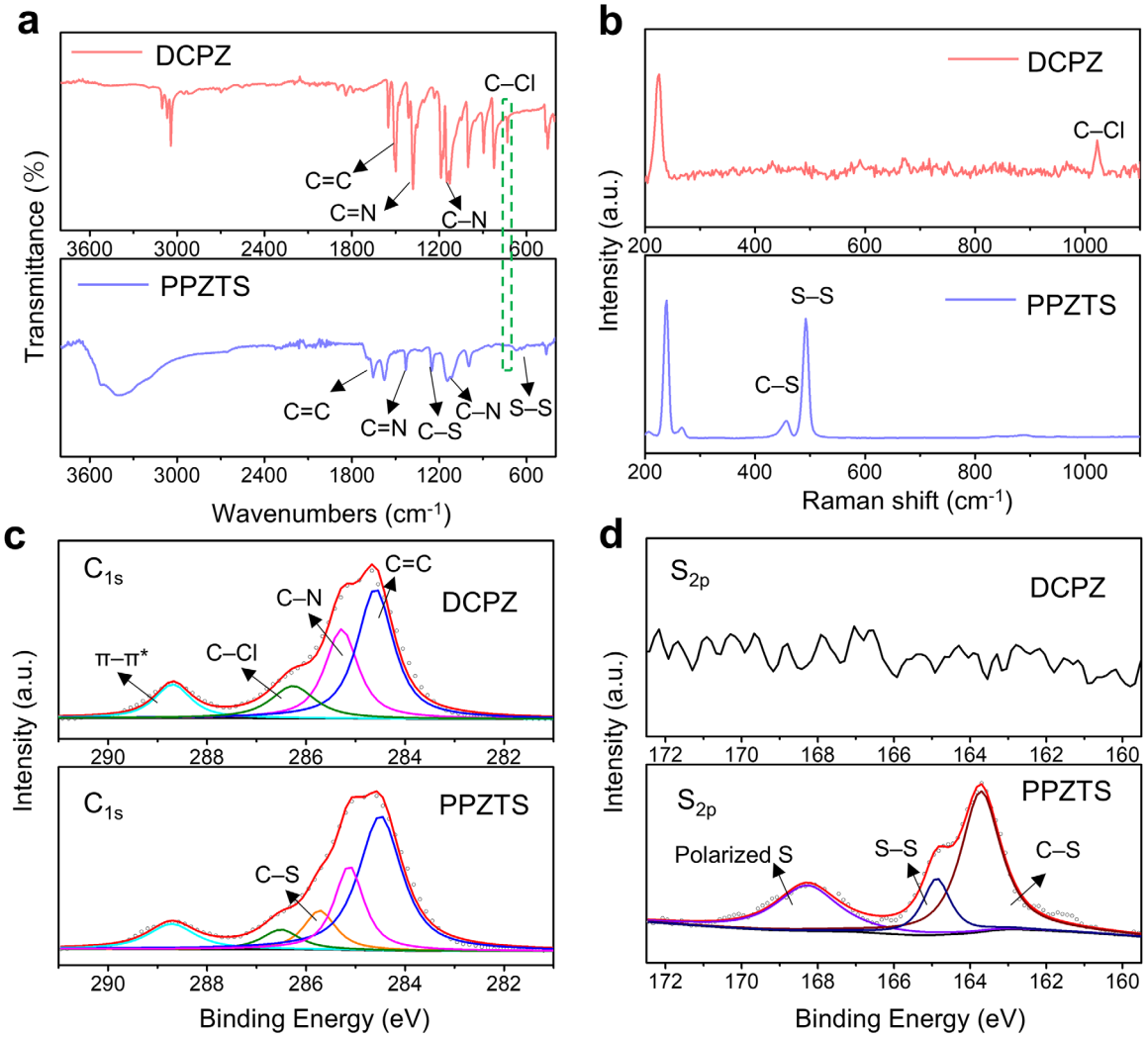

FIGURE 2 | Spectroscopic characterizations of DCPZ precursor and PPZTS. (a) FTIR spectra, (b) Raman spectra, and (c, d) XPS spectra at (c) C 1s and (d) S 2p regions of DCPZ precursor and PPZTS, respectively.

cathode also increases, and the redox peaks are kept intact. This indicates that the PPZTS cathode has good kinetic performance and electrochemical reversibility.

To more quantitatively evaluate the electrochemical kinetics of PPZTS cathode, fitted straight lines were obtained by fitting the peak currents of CV curves vs. the square roots of scan rates (Figure 3d), and the diffusion coefficient of lithium ions was calculated according to the Randles-Sevcik formula: [37]

$$I_p = 2.65 \times 10^5 n^{1.5} S D_{Li^+}{}^{0.5} C v^{0.5} \quad (1)$$

where *Ip* is the peak current (A mg^{-1}), *n* is the charge transfer number, *S* is the area of the electrode (cm^2), $D_{Li}{}^+$ is the diffusion coefficient of Li^+ ($cm^2\ s^{-1}$), and *C* is the volumetric concentration of Li^+ in the electrolyte (mol cm^{-3}), and *v* is the scan rate (V s^{-1}). Since the influencing factors of the slopes of the fitting lines are all constants except for $D_{Li}{}^+$, the slope is only related to the diffusion coefficient of Li^+. Compared with traditional S/C cathode (Figure S3), the slopes of the fitted straight lines of PPZTS cathode are larger (as presented in Table S2), and the calculated $D_{Li}{}^+$ values are summarized in Table S3. This indicates a higher Li^+ diffusion coefficient, further verifying the enhanced Li-ion diffusion kinetics of PPZTS cathode. Furthermore, the Li-ion diffusion coefficient ($D_{Li}{}^+$) of PPZTS cathode was determined with galvanostatic intermittent titration technique (GITT) (Figure S4), demonstrating elevated Li-ion diffusion capability for PPZTS in the range of 10^{-7}–10^{-10} $cm^2\ s^{-1}$ relative to conventional S/C material (10^{-10}–10^{-12} $cm^2\ s^{-1}$) [37].

The electrochemical performances of PPZTS cathode in lithium-organosulfide batteries were comprehensively measured (Figure 4). The rate test results of PPZTS cathode (Figure 4a) demonstrate a high specific capacity of 1250 mAh g^{-1} at 0.1 A g^{-1} and an excellent capacity retention of at 660 mAh g^{-1} at 5.0 A g^{-1}, underscoring its potential for use in high-rate applications. As a comparison, Figure S5a shows the rate performance of the traditional S/C cathode. When the current density reaches 5.0 A g^{-1}, its discharge specific capacity is only about 270 mAh g^{-1}. The utilization percentages of PPZTS cathodes remain consistently higher than that of S/C cathodes across different current densities, clearly demonstrating the superior rate performance of PPZTS cathodes (Table S4). The galvanostatic discharge/charge profiles of PPZTS cathode at different current

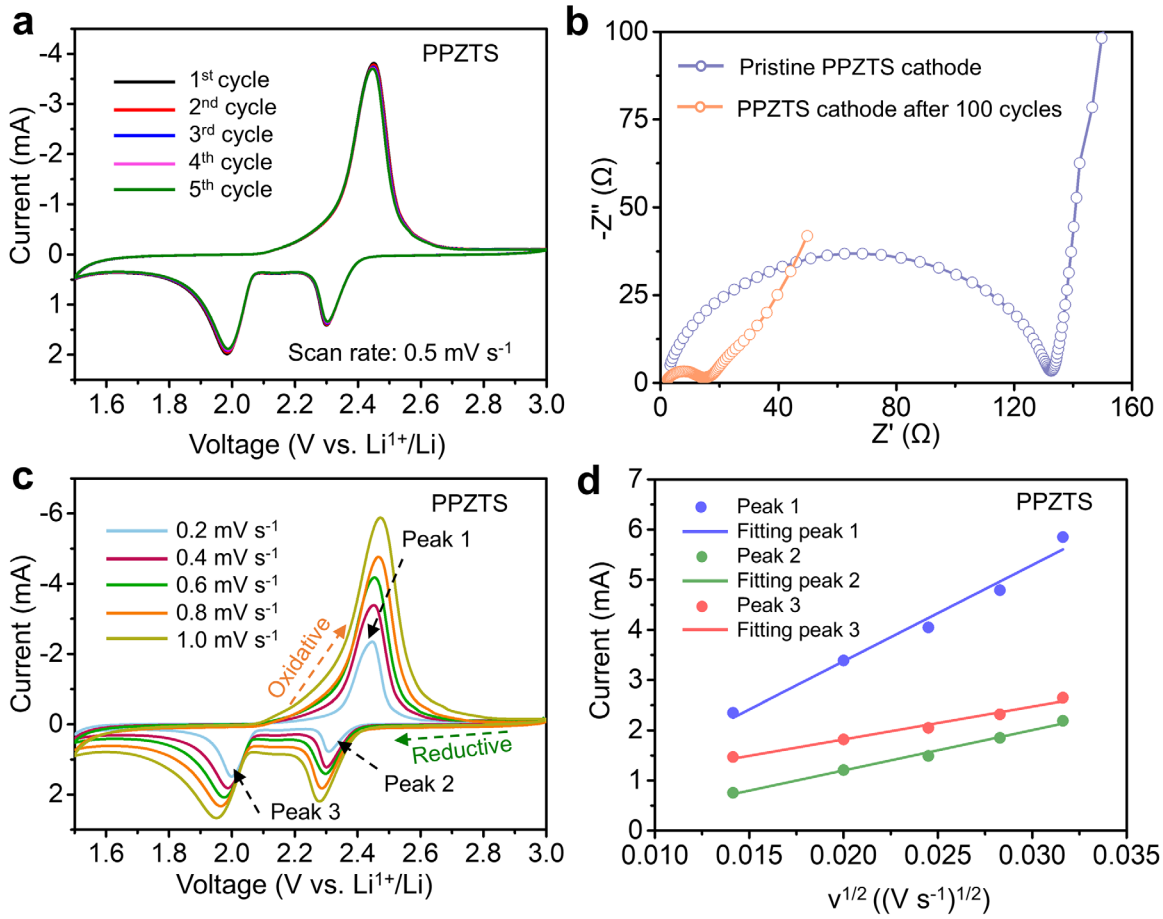

FIGURE 3 | Electrochemical kinetic properties of PPZTS cathode. (a) CV curves of PPZTS cathode at a scan rate of 0.5 mV s^{-1} in the voltage range of 1.5–3.0 V vs. Li^+/Li. (b) EIS spectrum of PPZTS cathode at pristine state and after 100 cycles. (c) CV curves of PPZTS cathode at various scan rates from 0.2 to 1.0 mV s^{-1}. (d) The fitted plots of CV peak currents vs. the square roots of scan rates ($v^{1/2}$) obtained from (c).

densities (Figure 4b) reveal stable voltage plateaus, indicating excellent electrochemical reaction kinetics.

The temperature-variated cycle performance tests suggest that the good high and low temperature durability of PPZTS cathode (Figure 4c; Table S5). Under low-temperature conditions of −20 and 0°C, the PPZTS cathode demonstrates specific capacities of 333 and 565 mAh g^{-1}, respectively. When the temperature raises from room temperature to 80°C, the specific capacity of PPZTS cathode increases from 750 to 1100 mAh g^{-1}. At an elevated temperature of 80°C, the battery still maintains a capacity of 890 mAh g^{-1} after 30 cycles (Figure S6). The excellent kinetics and structural integrity, stemming from the conjugated pyrazine backbone and short S_4 chains, underpin this wide-temperature capability. The galvanostatic discharge/charge profiles of PPZTS cathode between −20 and 80°C also demonstrate stable voltage plateaus (Figure 4d), indicating the working stability of PPZTS cathode over a wide temperature range, which is crucial for practical application.

The long-term cycling test of PPZTS cathode at 1.0 A g^{-1} (Figure 4e) demonstrates an initial capacity of 850.9 mAh g^{-1} and well preserves a value of 630.4 mAh g^{-1} after 400 cycles, corresponding to an ultralow average capacity decay rate of only 0.075% per cycle, underscoring its considerable promise for extended operational lifespans. Conversely, the traditional S/C cathode demonstrates inadequate stability during prolonged cycling, manifesting a capacity of merely 335mAh g^{-1} after 400 cycles at 1.0 A g^{-1} (Figure S5b), corresponding to a higher capacity decay rate of 0.13% per cycle. At a high current density of 5.0 A g^{-1}, the PPZTS cathode still shows a high capacity and cycling stability (Figure S8).

The areal loading and electrolyte dosage are also pivotal parameters for the evaluation of battery material feasibility. As presented in Figure S9, a heightened PPZTS loading (4.1 mg cm^{-2}) and a limited electrolyte supply (4 μL mg_{PPZTS}^{-1}) were applied for testing the cycling performance. The Li||PPZTS battery with a low electrolyte-to-sulfur (E/S) ratio of 6 μL mg_S^{-1} sustains a specific capacity of 671.5 mAh g^{-1} and an areal capacity of 559.6 mAh cm^{-2} over 70 cycles at a current density of 1.0 A g^{-1}, demonstrating efficient and stable performance under stringent operating conditions.

The practical potential of PPZTS cathode was further evaluated by the assembly and tests of soft-packed Li||PPZTS battery (Figure 4f,g). The soft-packed Li||PPZTS battery delivers an initial capacity of 820 mAh g^{-1} at 1.0 A g^{-1} and retains at 479.5 mAh g^{-1} after 90 cycles. For the soft-packed Li||PPZTS battery (Figure 4g), its gravimetric energy density is calculated to be 233.9 Wh kg^{-1}

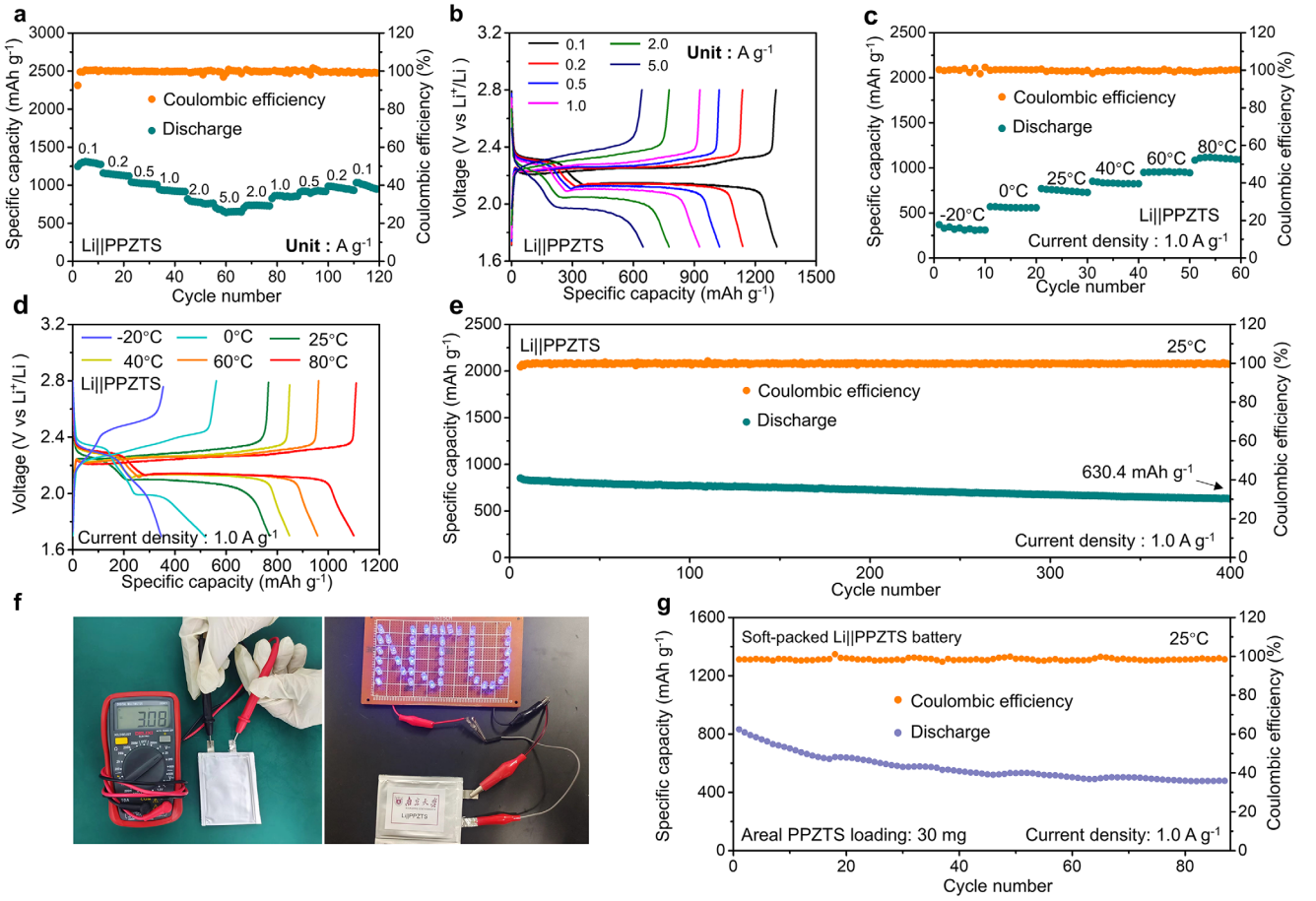

FIGURE 4 | Electrochemical performances of PPZTS cathode. (a) Rate capability and (b) corresponding galvanostatic discharge/charge profiles of PPZTS cathodes tested at various current densities from 0.1 to 5.0 A g^{-1}. (c) Temperature-dependent capacity variation and (d) corresponding galvanostatic discharge/charge profiles of PPZTS cathodes at various temperatures from −20 to 80°C at a current density of 1.0 A g^{-1}. (e) Long-term cycling performance of PPZTS cathode at a current density of 1.0 A g^{-1}. (f) A LED lamp grid steadily powered by a soft-packed Li||PPZTS battery. (g) Cycling performance and Coulombic efficiency of the soft-packed Li||PPZTS battery tested at 1.0 A g^{-1}.

(with the key parameters and performances summarized in Table S6), demonstrating the practical application potential of PPZTS cathodes in realistic battery configurations. Pre- and post-cycling examinations reveal that the morphological features of PPZTS cathode before and after long cycling remain almost identical (Figure S10), underscoring its good structural stability.

To delve into the underlying working mechanism of PPZTS cathode, the PPZTS cathodes in the batteries at different discharge/charge states were disassembled after a specified number of cycles and underwent ex situ analyses involving XPS, Raman, and UV–vis characterizations. The primary objective is to elucidating the Li^+ storage mechanism and ascertaining the extent of polysulfide formation during cycling. After 100 cycles, the C1s and S2p XPS spectra of PPZTS cathode upon discharged to 2.25 and 1.70 V are displayed in Figure 5a–b, respectively. At a cutoff voltage of 2.25 V, a distinct C–S peak is consistently detected at 285.6 eV, signifying the characteristic bonding between carbon and sulfur (Figure 5a) [36, 38]. As the discharge process progresses to 1.70 V, the intensity of C–S peak obviously decreases. This phenomenon is indicative of the formation of C–S–S-Li and subsequent C–S–Li structures due to the reaction of Li^+ with the C–S_4–C moieties, leading to signal attenuation. In parallel, the evolution of N 1s spectra (Figure S11) demonstrates the dynamic chemical interaction between the polar N sites and lithium polysulfides, which synergistically facilitates the immobilization and conversion of intermediates. The S 2p XPS spectrum presented in Figure 5b delineates the formation of lithiated species like C–S–S–Li at 2.25 V, denoted by the peak at 163.5 eV [39]. Upon discharged to 1.70 V, the C–S–S–Li species have made a complete transformation into C–S–Li and Li_2S, leading to the disappearance of the peak at 163.5 eV. Additionally, SEM images and corresponding elemental mappings of PPZTS cathode at discharge voltage of 2.25 V and 1.70 V are shown in Figures S12 and S13. The homogeneous distributions of S and N elements at different states indicated that PPZTS active material is well preserved and would not dissolve in the electrolyte, thereby overcoming the shuttle effect.

Ex situ Raman spectroscopy (Figure 5c) was employed to validate the charge-discharge steps of PPZTS cathodes after 100 cycles. During the discharge phase, distinct signals corresponding to C–S–S-Li and C–S–Li structures initially appeared in the range of 1000–1090 cm^{-1}, succeeded by the emergence of the Li_2S_2 signal at 750 cm^{-1} [40, 41]. As discharge voltage decreases, the intensities of these signals associated with short sulfur-chain

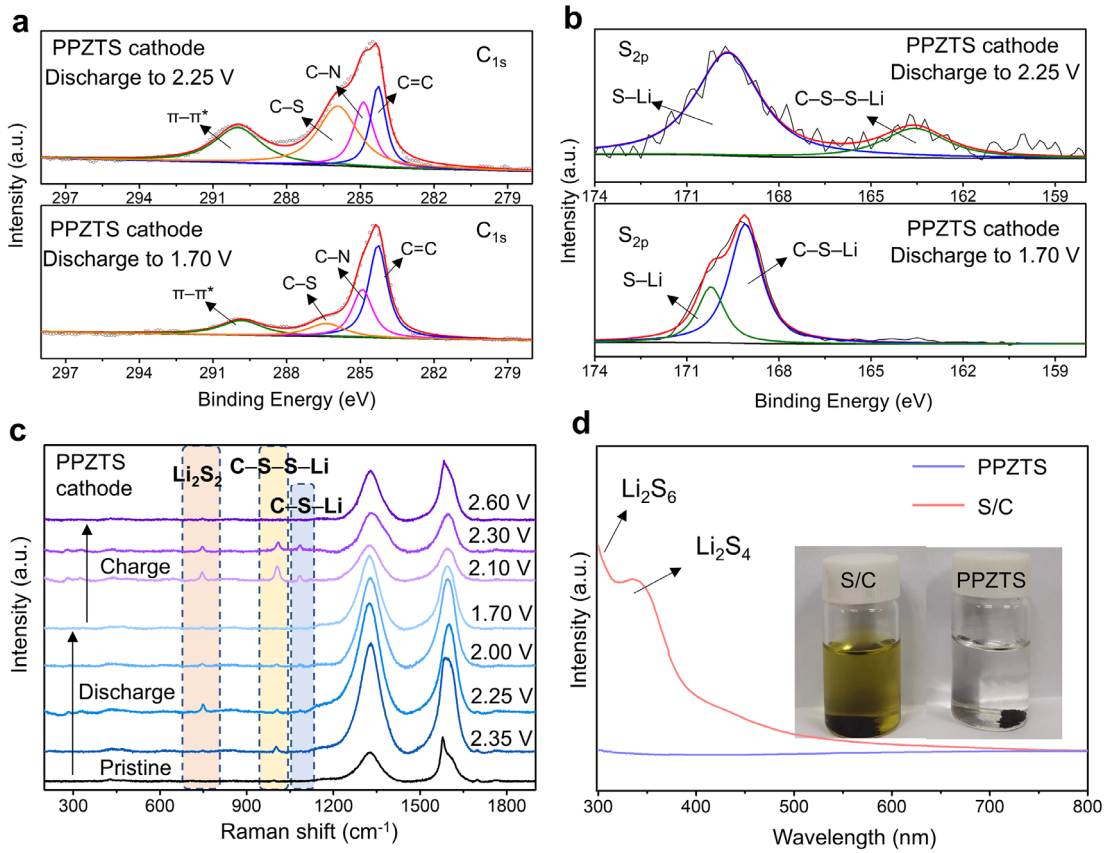

FIGURE 5 | Working mechanism studies of PPZTS cathode. (a, b) XPS spectra at (a) C1s and (b) S2p regions of PPZTS cathode after discharged to 2.25 and 1.70 V, respectively. (c) Ex situ Raman spectra of PPZTS electrode at pristine state and various discharge/charge states. (d) UV–vis absorption spectra and (the inset) corresponding photograph of DME solutions soaked with PPZTS and traditional S/C cathodes after discharged to 2.25 V.

species dwindle and finally disappear upon full discharge. This stepwise transformation of sulfur species during discharge aligns well with the two reduction peaks observed in the CV curve of PPZTS cathode, further confirming the progressive electrochemical reduction process. Notably, the signals of S_4^{2-} and S_6^{2-} species are totally absent during the entire process. Furthermore, ex situ XRD analysis of the deeply discharged cathode (Figure S14) directly confirmed the formation of crystalline Li_2S as the final discharge product, providing definitive structural evidence for the solid-phase endpoint of this reduction pathway. In the charge phase, the simultaneous manifestation of C–S–S–Li, C–S–Li and Li_2S_2 signals corresponded to the solitary oxidation peak is discernible in the Raman spectra. As the charge process ends, these characteristic signal peaks disappear.

To further assess the cycling stability of PPZTS active material, the disassembled PPZTS and traditional S/C electrodes after 400 cycles were immersed in a dimethoxyethane (DME) solution for UV–vis spectroscopic characterizations (Figure 5d). For reference, standard Li_2S_6 solutions with different concentrations were measured, confirming that characteristic polysulfide absorption features are detectable down to an extremely low concentration level of 10^{-9} M (Figure S15). The traditional S/C electrode exhibits two prominent absorption peaks at 300 and 450–500 nm, corresponding to the characteristic absorption of Li_2S_6 and Li_2S_4, respectively, confirming the dissolution of polysulfide species in the electrolyte [37]. In contrast, the PPZTS electrode-soaked solution shows no noticeable absorption peak, indicating the absence of dissolved polysulfides and demonstrating the avoidance of polysulfide formation [42, 43]. The inset of Figure 5d visually depicted the almost colorless PPZTS electrode-soaked solution, in comparison with the dark yellow color of the traditional S/C electrode-soaked solution. Following the drying process of the immersed electrodes, SEM and EDX analyses were executed (Figure S16), revealing a more concentrated distribution of S element in the cycled PPZTS electrode, indicative of the improved active substance preservation and capacity retention. In contrast, the distribution of sulfur species on traditional S/C cathodes appears sparser, hinting the loss of active substance due to the shuttle effect. This difference is further supported by the atomic ratio of C to S, measured at 1:1.02 in the cycled PPZTS electrode and only 1:0.26 in the S/C cathode, revealing a significant sulfur loss in the latter sample. These results highlight the enhanced ability of the PPZTS framework to retain sulfur species and suppress their migration, thereby contributing to improved structural stability and electrochemical performance among reported organosulfur cathodes [44–50].

3 | Conclusion

In summary, we propose heterocycle-bridged short sulfur-chain polymers as a class of effective cathode materials for lithium-organosulfide batteries. The distinctive structure of PPZTS, featuring a pyrazine-bridged short sulfur-chains, not only inhibits the generation of polysulfides but also enhances lithium sulfide

adsorption, leading to improved rate capability and cycling life. The PPZTS cathode exhibits favourable rate performance at various current densities, delievering a specific capacity of 1250 mAh g^{-1} at 0.1 A g^{-1} and 660 mAh g^{-1} at 5.0 A g^{-1}. Moreover, a high initial capacity of 850.9 mAh g^{-1} is achieved at 1.0 A g^{-1}, and retains a value of 630.4 mAh g^{-1} after 400 cycles. Additionally, the PPZTS cathode demonstrates high robustness and durability across a wide temperature range, maintaining 1100 mAh g^{-1} at 80°C and 330 mAh g^{-1} at −20°C. The application in soft-packed batteries further confirms its practical application potential. Comprehensive characterization and mechanism studies reveal that the PPZTS cathode stores Li^+ through a reversible transformation of C–S, C–S–S–Li, and C–S–Li bonds, accompanied by the stepwise conversion of short-chain sulfur species. This well-regulated reaction pathway effectively prevents the formation and shuttling of long-chain polysulfides, thereby ensuring structural integrity and stable cycling performance. This work highlights the immense potential of heterocycle-bridged short sulfur-chain polymers as advanced cathode materials in alkali metal-sulfur batteries, offering a promising pathway for resolving critical constraints that have limited organosulfur polymer deployment in advanced energy storage systems.

Acknowledgements

This work was supported by the National Natural Science Foundation of China (U25A20628, 22561160129, 22479074, 22475096), the Equipment Pre-Research and Ministry of Education Joint Fund (8091B02052407), the Fundamental Research Program Key Project of Jiangsu Province (BK20253008), the Science and Technology Major Project of Jiangsu Province (BG2024013), the Scientific and Technological Achievements Transformation Special Fund of Jiangsu Province (BA2023037), the Academic Degree and Postgraduate Education Reforming Project of Jiangsu Province (JGKT24_C001), the Key Core Technology Open Competition Project of Suzhou City (SYG2024122), the Open Research Fund of Suzhou Laboratory (SZLAB-1308-2024-TS005), and the Chenzhou National Sustainable Development Agenda Innovation Demonstration Zone Provincial Special Project (2023sfq11).

Author Contributions

Z. J. and X. M. conceived the idea for this study, with X. M. responsible for the preparation of materials. FTIR, Raman, and XPS analyses were carried out by X. M., H. L., and T. S., while electrochemical measurements were performed by X. M., Y. W., and X. S. Data analysis was conducted by X. M., T. S., J. L., Z. W., H. W., L. Q., T. Y., and Z. T. Z. J. and X. M. analyzed the results and wrote the manuscript, which was revised by Z. J., who also supervised the project. All authors discussed the results and commented on the manuscript.

Conflicts of Interest

The authors declare no conflicts of interest.

Data Availability Statement

The data that support the findings of this study are available from the corresponding author upon reasonable request.

References

1. Y. Liu, S. Liu, G. R. Li, and X. P. Gao, "Strategy of Enhancing the Volumetric Energy Density for Lithium–Sulfur Batteries," *Advanced Materials* 33 (2021): 2003955, https://doi.org/10.1002/adma.202003955.

2. L. Wang, X. Yin, C. Jin, C. Lai, G. Qu, and G. Zheng, "Cathode-Supported-Electrolyte Configuration for High-Performance all-Solid-State Lithium-Sulfur Batteries," *ACS Applied Materials & Interfaces* 3 (2020): 11540–11547, https://doi.org/10.1021/acsaem.0c02347.

3. C. Zhao, G. Xu, Z. Yu, et al., "Author Correction: A high-energy and long-cycling lithium–sulfur pouch cell via a macroporous catalytic cathode With double-end binding sites," *Nature Nanotechnology* 16 (2021): 224–224, https://doi.org/10.1038/s41565-020-00797-w.

4. Z. Liang, D. Yang, P. Tang, et al., "Atomically dispersed Fe in a C 2 N Based Catalyst as a Sulfur Host for Efficient Lithium–Sulfur Batteries," *Advanced Energy Materials* 11 (2021): 2003507, https://doi.org/10.1002/aenm.202003507.

5. Z. Wang, Y. Dong, H. Li, et al., "Enhancing lithium–sulphur battery performance by strongly binding the discharge products on amino-functionalized reduced graphene oxide," *Nature Communications* 5 (2014): 5002, https://doi.org/10.1038/ncomms6002.

6. Y. Ren, B. Wang, H. Liu, et al., "CoP Nanocages Intercalated MXene Nanosheets as a Bifunctional Mediator for Suppressing Polysulfide Shuttling and Dendritic Growth in Lithium-sulfur Batteries," *Chemical Engineering Journal* 450 (2022): 138046, https://doi.org/10.1016/j.cej.2022.138046.

7. Y. Xiao, Y. Xiang, S. Guo, et al., "An Ultralight Electroconductive Metal-organic Framework Membrane for Multistep Catalytic Conversion and Molecular Sieving in Lithium-sulfur Batteries," *Energy Storage Materials* 51 (2022): 882–889, https://doi.org/10.1016/j.ensm.2022.07.018.

8. B. Jin, L. Yang, J. Zhang, et al., "Bioinspired Binders Actively Controlling Ion Migration and Accommodating Volume Change in High Sulfur Loading Lithium–Sulfur Batteries," *Advanced Energy Materials* 9 (2019): 1902938, https://doi.org/10.1002/aenm.201902938.

9. L. Ma, G. Zhu, W. Zhang, et al., "Three-dimensional Spongy Framework as Superlyophilic, Strongly Absorbing, and Electrocatalytic Polysulfide Reservoir Layer for High-rate and Long-cycling Lithium-sulfur Batteries," *Nano Research* 11 (2018): 6436–6446, https://doi.org/10.1007/s12274-018-2168-8.

10. M. Li, J. Lu, and Z. Chen, "30 Years of Lithium-Ion Batteries," *Advanced Materials* 30 (2018): 1800561, https://doi.org/10.1002/adma.201800561.

11. A. Eftekhari, "High-Energy Aqueous Lithium Batteries," *Advanced Energy Materials* 8 (2018): 81801156, https://doi.org/10.1002/aenm.201801156.

12. S. Chen, J. Zheng, L. Yu, et al., "High-Efficiency Lithium Metal Batteries With Fire-Retardant Electrolytes," *Joule* 2 (2018): 1548–1558, https://doi.org/10.1016/j.joule.2018.05.002.

13. Y. Cai, J. Zhou, G. Fang, G. Cai, A. Pan, and S. Liang, "Na0.282V2O5: A high-performance cathode material for rechargeable lithium batteries and sodium batteries," *Journal of Power Sources* 328 (2016): 241–249, https://doi.org/10.1016/j.jpowsour.2016.08.016.

14. F. Wan, L. Fang, X. Zhang, C. A. Wolden, and Y. Yang, "Lithium Sulfide Nanocrystals as Cathode Materials for Advanced Batteries," *Journal of Energy Chemistry* 63 (2021): 138–169, https://doi.org/10.1016/j.jechem.2021.09.028.

15. H. Shuai, J. Li, W. Hong, et al., "Electrochemically Modulated LiNi 1/3 Mn 1/3 Co 1/3 O 2 Cathodes for Lithium-Ion Batteries," *Small Methods* 3 (2019): 1900065, https://doi.org/10.1002/smtd.201900065.

16. Y. Lyu, X. Wu, K. Wang, et al., "An Overview on the Advances of LiCoO 2 Cathodes for Lithium-Ion Batteries," *Advanced Energy Materials* 11 (2021): 2000982, https://doi.org/10.1002/aenm.202000982.

17. J. Zheng, G. Ji, X. Fan, et al., "High-Fluorinated Electrolytes for Li–S Batteries," *Advanced Energy Materials* 9 (2019): 1803774, https://doi.org/10.1002/aenm.201803774.

18. J. Zheng, X. Fan, G. Ji, et al., "Manipulating Electrolyte and Solid Electrolyte Interphase to Enable Safe and Efficient Li-S Batteries," *Nano Energy* 50 (2018): 431–440, https://doi.org/10.1016/j.nanoen.2018.05.065.

19. Y. X. Yin, S. Xin, Y. G. Guo, and L. J. Wan, "Lithium–Sulfur Batteries: Electrochemistry, Materials, and Prospects," *Angewandte Chemie International Edition* 52 (2013): 13186–13200, https://doi.org/10.1002/anie.201304762.

20. R. Fang, S. Zhao, Z. Sun, D. W. Wang, H. M. Cheng, and F. Li, "More Reliable Lithium-Sulfur Batteries: Status, Solutions and Prospects," *Advanced Materials* 29 (2017): 1606823, https://doi.org/10.1002/adma.201606823.

21. Y. C. Jeong, J. H. Kim, S. Nam, C. R. Park, and S. J. Yang, "Rational Design of Nanostructured Functional Interlayer/Separator for Advanced Li–S Batteries," *Advanced Functional Materials* 28 (2018): 1707411, https://doi.org/10.1002/adfm.201707411.

22. L. Huang, J. Li, B. Liu, et al., "Electrode Design for Lithium–Sulfur Batteries: Problems and Solutions," *Advanced Functional Materials* 30 (2020): 1910375, https://doi.org/10.1002/adfm.201910375.

23. C. Fu and J. Guo, "Challenges and current development of sulfur cathode in lithium–sulfur battery," *Current Opinion in Chemical Engineering* 13 (2016): 53–62, https://doi.org/10.1016/j.coche.2016.08.004.

24. C. Hu, H. Chen, Y. Shen, et al., "In Situ Wrapping of the Cathode Material in Lithium-sulfur Batteries," *Nature Communications* 8 (2017): 479, https://doi.org/10.1038/s41467-017-00656-8.

25. M. Yu, R. Li, Y. Tong, et al., "A graphene wrapped hair-derived carbon/sulfur composite for lithium–sulfur batteries," *Journal of Materials Chemistry A* 3 (2015): 9609–9615, https://doi.org/10.1039/c5ta00651a.

26. M. Li, Z. Chen, T. Wu, and J. Lu, "Li2S- or S-Based Lithium-Ion Batteries," *Advanced Functional Materials* 30 (2018): 1801190, https://doi.org/10.1002/adma.201801190.

27. W. Zhou, C. Wang, Q. Zhang, et al., "Tailoring Pore Size of Nitrogen-Doped Hollow Carbon Nanospheres for Confining Sulfur in Lithium–Sulfur Batteries," *Advanced Energy Materials* 5 (2015): 1401752, https://doi.org/10.1002/aenm.201401752.

28. J. Song, T. Xu, M. L. Gordin, et al., "Nitrogen-Doped Mesoporous Carbon Promoted Chemical Adsorption of Sulfur and Fabrication of High-Areal-Capacity Sulfur Cathode With Exceptional Cycling Stability for Lithium-Sulfur Batteries," *Advanced Functional Materials* 24 (2014): 1243–1250, https://doi.org/10.1002/adfm.20130263.

29. P. Sang, J. Song, W. Guo, and Y. Fu, "Hyperbranched Organosulfur Polymer Cathode Materials for Li-S Battery," *Chemical Engineering Journal* 415 (2021): 129043, https://doi.org/10.1016/j.cej.2021.129043.

30. Y.-H. Liu, W. Chang, J. Qu, et al., "A Polymer Organosulfur Redox Mediator for High-performance Lithium-sulfur Batteries," *Energy Storage Materials* 46 (2022): 313–321, https://doi.org/10.1016/j.ensm.2022.01.021.

31. Z. Jiang, H. J. Guo, Z. Zeng, et al., "Reconfiguring Organosulfur Cathode by Over-Lithiation to Enable Ultrathick Lithium Metal Anode Toward Practical Lithium–Sulfur Batteries," *ACS Nano* 14 (2020): 13784–13793, https://doi.org/10.1021/acsnano.0c06133.

32. Z. Pan, D. J. L. Brett, G. He, and I. P. Parkin, "Progress and Perspectives of Organosulfur for Lithium–Sulfur Batteries," *Advanced Energy Materials* 12 (2022): 2103483, https://doi.org/10.1002/aenm.202103483.

33. W. Guo, D. Y. Wang, Q. Chen, and Y. Fu, "Advances of Organosulfur Materials for Rechargeable Metal Batteries," *Advanced Science* 9 (2022): 2103989, https://doi.org/10.1002/advs.202103989.

34. X. Li, L. Yuan, D. Liu, et al., "High Sulfur-containing Organosulfur Polymer Composite Cathode Embedded by Monoclinic S for Lithium Sulfur Batteries," *Energy Storage Materials* 26 (2020): 570–576, https://doi.org/10.1016/j.ensm.2019.11.030.

35. Z. Wang, Q. Fan, Y. Si, W. Guo, and Y. Fu, "A Self-regulatory Organosulfur Copolymer Cathode towards High Performance Lithium-sulfur Batteries," *Energy Storage Materials* 58 (2023): 222–231, https://doi.org/10.1016/j.ensm.2023.03.020.

36. W. Chang, J. Qu, W. Li, et al., "Mesoporous Yolk-Shell Structured Organosulfur Nanotubes With Abundant Internal Joints for High-Performance Lithium–Sulfur Batteries by Kinetics Acceleration," *Small* 17 (2021): 2101857, https://doi.org/10.1002/smll.202101857.

37. A. Tao, K. Zhang, X. Ma, et al., "Building Lithium-Polycarbonsulfide Batteries With High Energy Density and Long Cycling Life," *ACS Energy Letters* 8 (2023): 79–89, https://doi.org/10.1021/acsenergylett.2c02107.

38. T. Sun, Z. J. Li, Y. F. Zhi, Y. J. Huang, H. J. Fan, and Q. Zhang, "Poly(2,5-Dihydroxy-1,4-Benzoquinonyl Sulfide) As an Efficient Cathode for High-Performance Aqueous Zinc–Organic Batteries," *Advanced Functional Materials* 31 (2021): 2010049, https://doi.org/10.1002/adfm.202010049.

39. H. Kang, H. Kim, and M. J. Park, "Sulfur-Rich Polymers With Functional Linkers for High-Capacity and Fast-Charging Lithium–Sulfur Batteries," *Advanced Energy Materials* 8 (2018): 1802423, https://doi.org/10.1002/aenm.201802423.

40. X. Zhang, G. Hu, K. Chen, et al., "Structure-related Electrochemical Behavior of Sulfur-rich Polymer Cathode With Solid-solid Conversion in Lithium-sulfur Batteries," *Energy Storage Materials* 45 (2022): 1144–1152, https://doi.org/10.1016/j.ensm.2021.11.014.

41. Y. Hu, W. Chen, T. Lei, et al., "Graphene Quantum Dots as the Nucleation Sites and Interfacial Regulator to Suppress Lithium Dendrites for High-loading Lithium-sulfur Battery," *Nano Energy* 68 (2020): 104373, https://doi.org/10.1016/j.nanoen.2019.104373.

42. R. Sun, Y. Bai, M. Luo, Z. Wang, W. Sun, and K. Sun, "Enhancing Polysulfide Confinement and Electrochemical Kinetics by Amorphous Cobalt Phosphide for Highly Efficient Lithium–Sulfur Batteries," *ACS Nano* 15 (2021): 739–750, https://doi.org/10.1021/acsnano.0c07038.

43. K. Chen, R. Fang, Z. Lian, et al., "An in-situ solidification strategy to block polysulfides in Lithium-Sulfur batteries," *Energy Storage Materials* 37 (2021): 224–232, https://doi.org/10.1016/j.ensm.2021.02.012.

44. Q. Pan; J. Lan; Y. Si; W. Guo, and Y. Fu, "A Fluorinated Macrocyclic Organodisulfide Cathode for Lithium Organic Batteries," *Chemical Communications* 58 (2022): 5602, https://doi.org/10.1039/d2cc00982j.

45. T. Zhang; F. Hu, W. Shao, et al., "Sulfur-Rich Polymers Based Cathode With Epoxy/Ally Dual-Sulfur-Fixing Mechanism for High Stability Lithium–Sulfur Battery," *ACS Nano* 15 (2021): 15027, https://doi.org/10.1021/acsnano.1c05330.

46. B. Long; J. Ma, T. Song, et al., "Bifunctional Polyvinylpyrrolidone Generates Sulfur-Rich Copolymer and Acts as "Residence" of Polysulfide for Advanced Lithium-Sulfur Battery," *Chemical Engineering Journal* 414 (2021): 128799, https://doi.org/10.1016/j.cej.2021.128799.

47. H. Hu; Y. Hu; H. Cheng; S. Dai; K. Song, and M. Liu, "Organic polysulfanes grafted on porous graphene as an electrode for high-performance lithium organosulfur batteries," *Journal of Power Sources* 491 (2021): 229617, https://doi.org/10.1016/j.jpowsour.2021.229617.

48. J. Zhou; X. Zhou; Y. Sun; X. Shen; T. Qian, and C. Yan, "Insight Into the Reaction Mechanism of Sulfur Chains Adjustable Polymer Cathode for High-Loading Lithium-Organosulfur Batteries," *Journal of Energy Chemistry* 56 (2021): 238, https://doi.org/10.1016/j.jechem.2020.08.010.

49. A. Bhargav and A. Manthiram, "A Lithium-Ion Conducting Polysulfide Polymer for Flexible Batteries," *ACS Mater Lett* 4 (2022): 1904–1911, https://doi.org/10.1021/acsmaterialslett.2c00590.

50. J. Kim; A. Elabd; S.-Y. Chung; A. Coskun, and J. W. Choi, "Covalent Triazine Frameworks Incorporating Charged Polypyrrole Channels for High-Performance Lithium–Sulfur Batteries," *Chemistry of Materials* 32 (2020): 4185, https://doi.org/10.1021/acs.chemmater.0c00246.

Supporting Information

Additional supporting information can be found online in the Supporting Information section.

Supporting file: aenm70688-sup-0001-SuppMat.docx